Check for updates

Research Article

Cycle Stability of Dual-Phase Lithium Titanate (LTO)/TiO₂ Nanowires as Lithium Battery Anode

Yillin Fan He*, Dongzhi Yang Chu, and Zhensheng Zhuo

Abstract

This work studied cycle stability of dual-phase lithium titanate (LTO)/TiO₂ nanowires as a lithium battery anode. Dual-phase LTO/TiO₂ nanowires were successfully synthesized by hydrothermal method at various times lithiation of 10, 24, and 48 h at 80 °C. SEM images show that the morphology of dual-phase LTO/TiO₂ is nanowires with a size around 100-200 nm in diameter. The XRD analysis result indicates nanowires main components are anatase (TiO₂) and spinel $Li_4Ti_5O_{12}$. The first discharge specific capacity of LTO/TiO₂-10, LTO/TiO₂-24, and LTO/TiO₂-48 was 181.68, 175.29, and 154.30 mAh/g, respectively. After the rate capacity testing, the LTO/TiO₂-10, LTO/TiO₂-24, and LTO/TiO₂-48 have been maintained at 161.25, 165.25, and 152.53 mAh/g separately. The retentions for each sample were 86.71, 92.86, and 89.79 %. Based on the results of electrochemical performance, increased LTO content helped increase samples cycle stability. However, the prolonged lithiation time also produced impurities, which reduced the cycle stability.

Keywords: anode, hydrothermal, lithium-ion battery, LTO-TiO₂, nanowires

1. INTRODUCTION

Nowadays, many electric and electronic devices have been developed, such as mobile phones, computer ignition, and lighting systems. With the growing power and durability of electric vehicles and portable electronic equipment, the production of high energy density batteries and reliable cycling efficiency is urgent [1][2]. Optimization of the batteries is one of the most significant methods. Among all practical batteries (lead-acid, nickel-cadmium, nickel-metal hydride, etc.), lithium ion batteries (LIBs) have effectively dominated the battery industry based on lithium intercalation chemistry and have essentially revolutionized our daily existence. Almost all of our mobile devices are powered by LIBs, and people want larger equipment, especially cars, to function better [3][4].

However, when it comes to the car scale, the traditional LIBs' ability cannot fully match the requirements. Currently, depending on the types of LIBs', there are one or more of the following problems: small specific capacity, low safety, low cycle life, high price, and low working temperature. Many improvement schemes are applied to the batteries, including modifying the electrode, improving electrolyte, developing the packaging technology, and so on [5]–[8].

In the process of exploring more suitable materials for LIBs anodes, Lithium titanate ($Li_4Ti_5O_{12}$ / LTO) has attracted tremendous attention due to its specific properties [9][10]. Compared with the commonly used graphite materials, it performs an operation voltage at around 1.55 V vs. Li⁺/Li, much higher than graphite (0.1 V vs. Li⁺/Li) [11]. It enables the $Li_4Ti_5O_{12}$ to avoid the self-discharge when working as an anode and thus enhances its safety and stability [12]. By comparing with other titanium-based anodes like TiO₂, the $Li_4Ti_5O_{12}$ shows higher cycle stability due to its "zero-strain" property, which means there is almost no volume change during the insertion and extraction of lithium-ions of the crystal [13][14]. On the other hand, as a precursor to producing LTO, theoretically TiO₂ possesses a specific capacity of 335 mAh/g, comparable to that of graphite [15]–[17]. Noerochim et al. [18] demonstrates that dual-phase LTO/TiO₂ has a high potential as anode material for high-rate application of LIBs.

The synthesized dual phase LTO/TiO₂ nanowire arrays have been applied as integrated anodes for high-rate LIBs [18]. The facile hydrothermal and ion exchange route developed to synthesize dual phase LTO/TiO₂ nanowire arrays. The resulting LTO/TiO₂ has a ratio of about 1:2. The introduction of TiO₂ to $Li_4Ti_5O_{12}$ increases the specific capacity
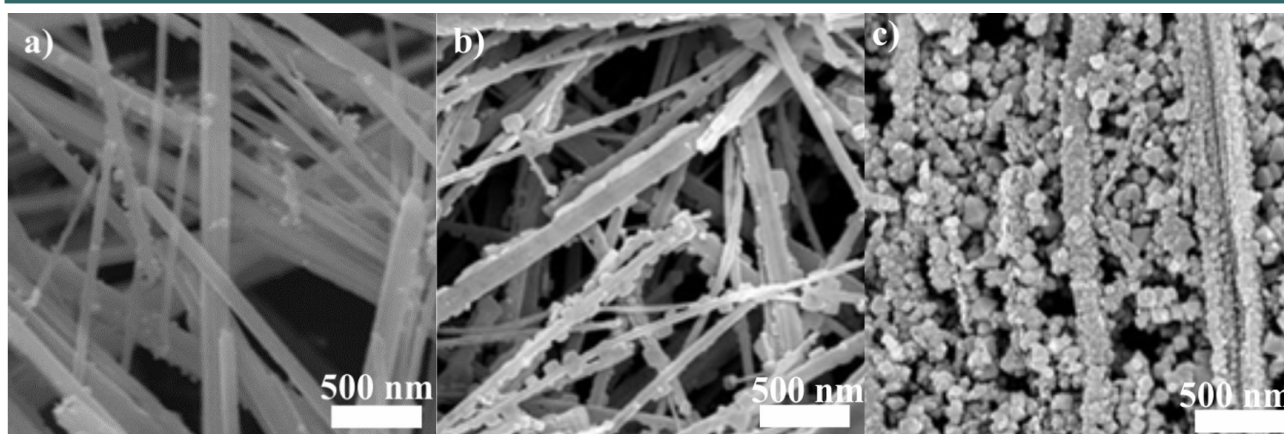
PANDAWA
INSTITUTE

Figure 1. SEM image of LTO/TiO$_2$-10 (a), LTO/TiO$_2$-24 (b), and LTO/TiO$_2$-48 (c)

and creates a dual-phase nanostructure with a high grain boundary density that facilitates electrons and Li-ions transport. The resulting dual-phase nanowire electrode has good rate capability compared to pure lithium titanate and TiO$_2$. The results obtained also explain that the dual-phase LTO/TiO$_2$ produced has good cycle stability.

In this work, the LTO-TiO$_2$ dual-phase nanowires synthesized using TiO$_2$ nanowires as precursors through a hydrothermal process at various times lithiation of 10, 24 and 48 h. SEM and XRD tests were carried out to characterize samples. The electrochemical tests were done through cycling and rate test to study the cycle stability.

2. MATERIALS AND METHODS

2.1. Materials

Laboratory grade titanium (IV) butoxide (97 %), glucose (≥99.5 %), ethanol, sodium hydroxide, hydrochloric acid and lithium hydroxide monohydrate purchased from Merck Sigma-Aldrich Reagent Pte, Singapore.

2.2. Methods

2.2.1. Hydrothermal synthesis LTO-TiO$_2$ nanowires

TiO$_2$ nanowires synthesized by a hydrothermal method. In this approach, 2 g titanium (IV) butoxide dissolved in 12 g ethanol. Sodium hydroxide (1.2 g) and 0.5 g glucose dissolved in 15 g water. These two solutions then mixed to form a white suspension. After stirring and ultrasonication, the suspension transferred to autoclave and heated to 260 ºC for 24 h. Afterwards, 2.5 mL hydrochloric acid (35 %) and 200 mL water added to the suspension. The suspension stood 24 h and washed with water and ethanol. After drying the product, the powders collected and calcined at 600 ºC with Ar protection for one h. The product then noted as TiO$_2$ nanowires.

To synthesize LTO/TiO$_2$ nanowires, the previous synthesized TiO$_2$ nanowires used as precursors. In this process, 0.05 g TiO$_2$ nanowires dispersed in water with the aid of ultrasonication. Then, 2.5 g lithium hydroxide monohydrate dissolved in the suspension. The suspension was transferred to an autoclave and heated to 80 ºC for

Table 1. Results of phase composition and structural parameters obtained from the Rietveld analysis.

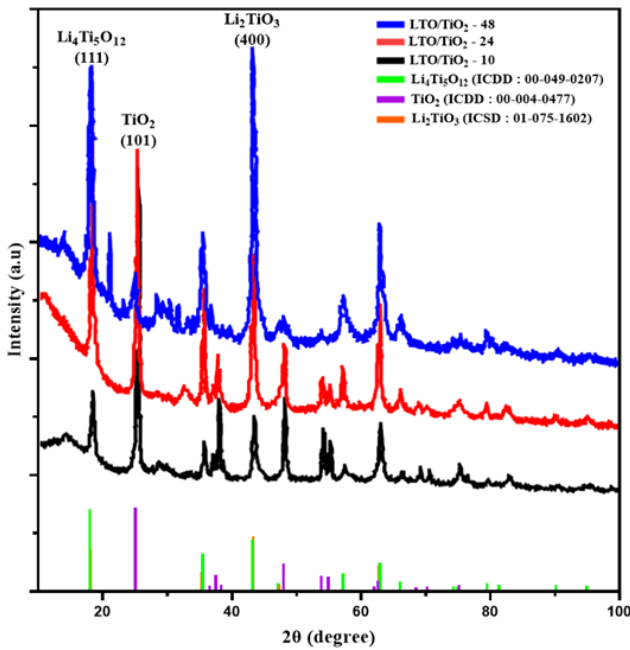| Sample	Phase	Composition (wt. %)	R$_p$	R$_{wp}$	χ^2
LTO/TiO$_2$-10	TiO$_2$	85.10	17.55	25.38	2.14
	LTO	14.90			
LTO/TiO$_2$-24	TiO$_2$	52.26	19.46	26.14	2.75
	LTO	45.74			
LTO/TiO$_2$-48	TiO$_2$	3.54	18.65	26.75	2.98
	LTO	78.50			
	Li$_2$TiO$_3$	17.96			

Figure 2. XRD patterns and peak patterns of LTO-TiO$_2$ nanowires with different lithiation time.

10 h, 24 h, and 48 h. After that, the product washed with water several times and then dried. Finally, the collected, dried white product annealed at a temperature of 600 ºC for 2 h and noted as LTO/TiO$_2$-10, LTO/TiO$_2$-24, and LTO/TiO$_2$-48.

2.2.2 LTO-TiO$_2$ Nanowires Characterization

LTO-TiO$_2$ nanowires that have produced are characterized using different instrument techniques. The surface morphology of nanoparticles studied using scanning electron microscopy (SEM, FEI Nova NanoSEM 450). The nanoparticles' crystal structure studied using X-ray diffraction (XRD, PANalytical Xpert Multipurpose X-ray Diffraction System) techniques. The range of 2θ set from 10 to 100, and the material for the target was cupper.

2.2.3. Electrochemical performance study

Li/Li$_2$O electrodes chosen as the counter electrode for the tested electrodes. 25 μm thick glass fibers used as the separators. The 1M lithium hexafluorophosphate in ethylene carbonate and ethyl methyl carbonate (5/5 by volume) selected as the electrolyte. All coin cells assembled in an Ar filled dry glove box.

The electrical properties analyzed by Netware CT-4008-5V10mA-164 batteries testing system, and the charge-discharge cycling performed between 1-3 V (vs Li/Li$^+$) at room temperature using different C rates (1 C=175 mA/g).
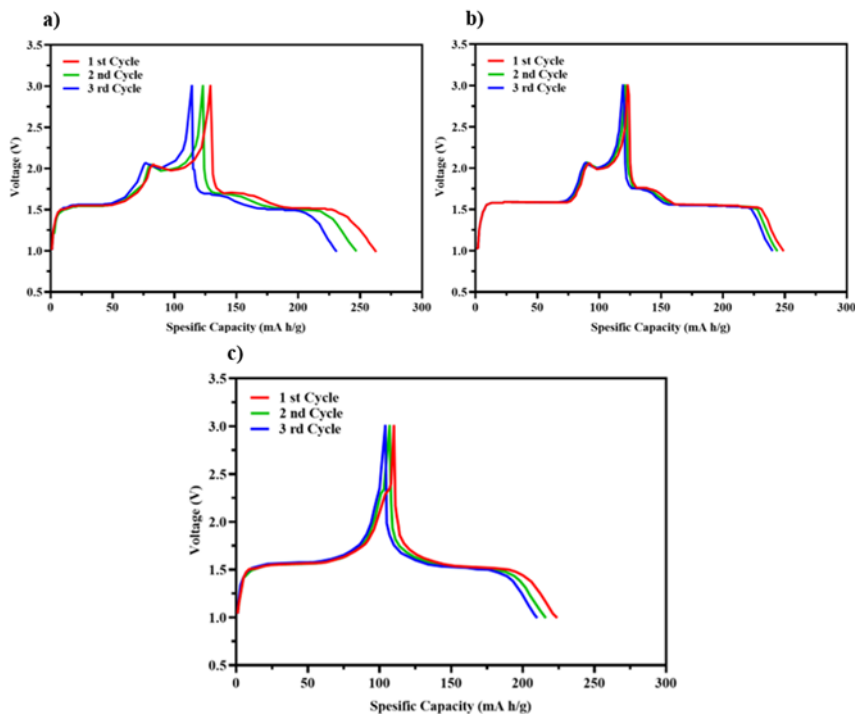

Figure 3. Charge-discharge curve of the initial 3 cycles of LTO/TiO$_2$-10 (a), LTO/TiO$_2$-24 (b), and LTO/TiO$_2$-48 (c).
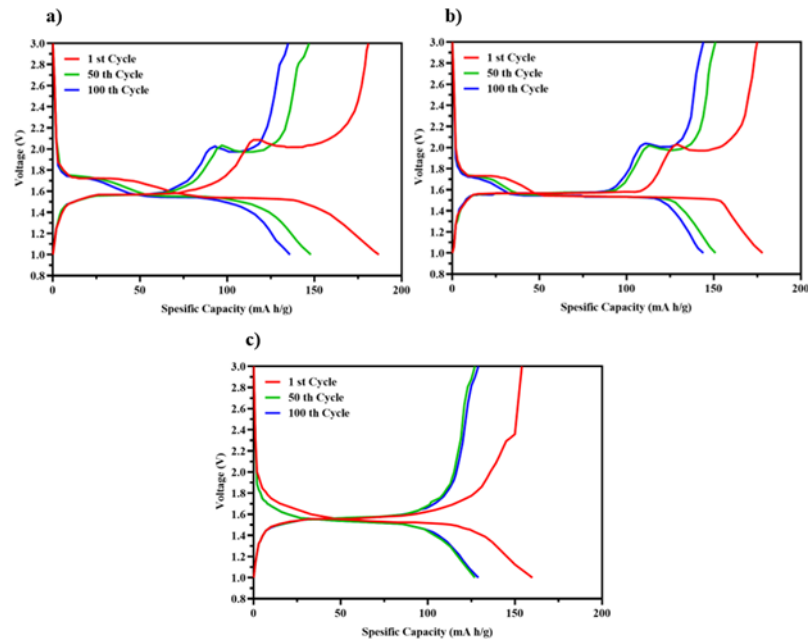
Figure 4. First, 50th and 100th voltage-specific capacity curves at 0.1 C of LTO/TiO$_2$-10 (a), LTO/TiO$_2$-24 (b), and LTO/TiO$_2$-48 (c)

3. RESULT AND DISCUSSIONS

3.1. SEM and XRD Characterization

The morphology of the nanowires examined with SEM. As shown in Figure 1 (a), after 10 h lithiation process, there were little small particles grown on the wires' surface. The mean diameter of nanowire samples determined from SEM imaging was around 100 nm. With the increasing of lithiation time, the amount of the small particles grew. After a 24 h reaction, the nanowires' structure can still be recognized (Figure 1 b). After 48 h reaction, most wires fully covered by the small lithiated particles (Figure 1 c). This process caused most of the separated nanowires to be connected and increased the nanowires diameter to around 200 nm. This phenomenon changed the morphology of the nanowires to more nanosheets-like or sponge-
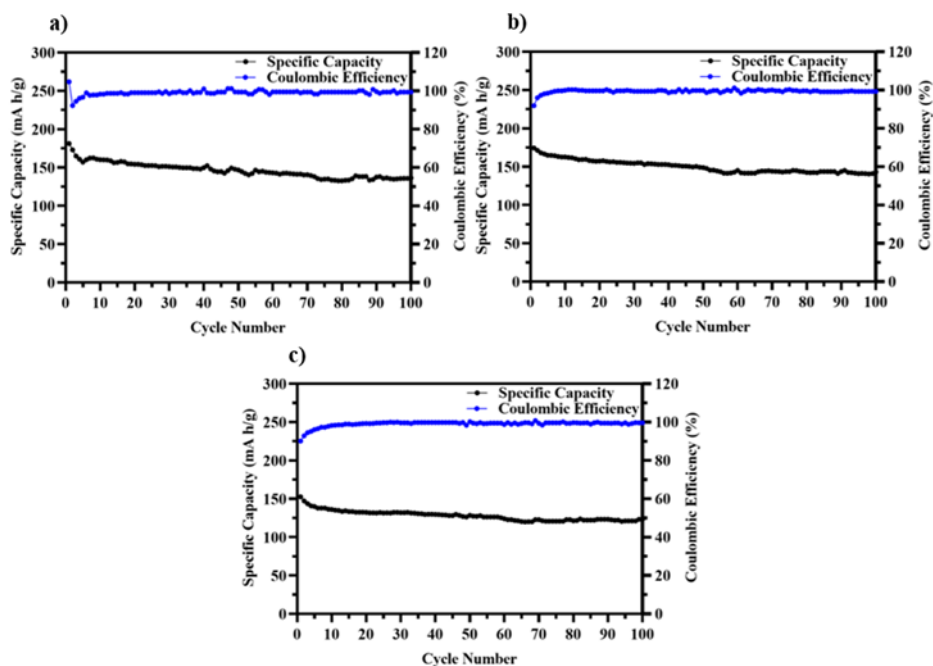

Figure 5. Cycling performance of LTO-TiO$_2$ nanowire. (a) LTO/TiO$_2$-10, (b) LTO/TiO$_2$-24, (c) LTO/TiO$_2$-48.

like structure [19].

XRD used to identify the crystallographic structure. As shown in Figure 2, after 10 h reaction, there a small number of $Li_4Ti_5O_{12}$ produced. However, a large number of TiO_2 phase remained. All major Bragg peaks well matched with those of anatase TiO_2 (ICDD no. 00-004-0477) [20] and cubic spinel $Li_4Ti_5O_{12}$ (ICDD no. 00-049-0207) [21] respectively. As the reaction time extends to 24 h, more TiO_2 phase consumed, and more LTO produced. The main components for the nanowires were still anatase TiO_2 and spinel $Li_4Ti_5O_{12}$ (Figure 2). After 48 h lithiation process, most TiO_2 reacted to form LTO. Because excessive LiOH was used as a lithium source during the hydrothermal reaction, the prolonged reaction enabled more lithium ions to be involved in the process [22].

Consequently, Li_2TiO_3 (ICSD no. 01-075-1602) [23] with a higher Li to Ti ratio than $Li_4Ti_5O_{12}$ was formed (Figure 2). The observed major peaks at 18.4437° and 43.2608° representatives for spinel $Li_4Ti_5O_{12}$, while the peak at 43.6510° contributed by (4 0 0) face of monoclinic Li_2TiO_3. Compared with 10 and 24 h samples, the major peak intensity for anatase TiO_2, which located at around 25.2872°, severely weakened, indicating the low content of TiO_2 in the nanowires. Also, the excessive lithium ions can be inserted into the lattice gaps in both Li_2TiO_3 and $Li_4Ti_5O_{12}$ to form LTO with different Li to Ti ratio. As a result, some miscellaneous peaks were observed in the XRD pattern (Figure 2). Unmatched peaks belongs to LTO with different phases. These XRD results confirm the SEM results where with increasing lithiation time, nanosheets-like or sponge-like structures are formed. The structure formed indicates the $Li_4Ti_5O_{12}$ produced during the process.

3.2. Electrochemical Characterization

Half-cell batteries tests carried out with metal lithium as both the counter and the reference electrode to study the electrochemical performance of all three kinds of dual-phase nanowires. Fig. 3 has shown the charge-discharge curves of the first three cycles of all three kinds of samples. During the charge and discharge process, the C rate was 0.5 C, so the current in this process a constant value for all three samples. All samples except LTO/TiO_2-48

display two distinguishable gradient changes during their charge and discharge processes (Figure 3 a, b). The turning points at around 2.0 V and 1.78 V referred to the insertion and extraction of lithium ions in the TiO_2 crystal. The turning points, which around 1.6 V and 1.5 V, on the other hand, were contributed by $Li_4Ti_5O_{12}$. In the batteries tests, capacity calculated by multiplication of time, current and voltage, since the current a fixed value, the area under the charge-discharge curve had represented the electrode's capacity. Naturally, a higher and longer plateau produces more capacity than a low and short plane [24].

In the case of LTO/TiO_2-48, there were no TiO_2 charge and discharge planes observed in its curve due to low TiO_2 content (Figure 3 c). $Li_4Ti_5O_{12}$ provided almost all capacity. As for the LTO/TiO_2-10, whose TiO_2 content was the highest, the curve shifted most (Figure 3 a). Both the charge and discharge planes of TiO_2 shortened while no significant variation happened to the $Li_4Ti_5O_{12}$ plane. The reason lies in the difference in electrochemical stability between these two contents. The $Li_4Ti_5O_{12}$ is known as zero strain materials in lithium-ion batteries, which means there is almost no volume change during the insertion and extraction of lithium ions [25]. Its crystal structure can be preserved to the greatest extent in the cyclic test. On the other hand, compared with $Li_4Ti_5O_{12}$, TiO_2 can store more lithium ions per formula unit. This property makes it inevitable that the crystal volume will change significantly in cycling. As a result, the crystal
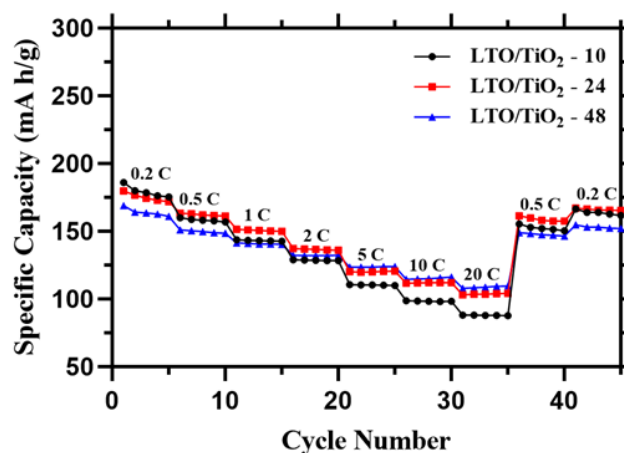

Figure 7. Rate performance at various current rate from 0.2 C to 20 C and then back to 0.5 C and 0.2 C of LTO/TiO_2-10, LTO/TiO_2-24, and LTO/TiO_2-48

structure is more likely to be damaged, and the capacity it provided is also reduced at a higher rate [26].

Figure 4 show the voltage-specific capacity curves at 0.1 C. As the cycle number increased, each sample had a decrease in both charge and discharged specific capacity. Considering the LTO/TiO_2-10 and the LTO/TiO_2-24 (Figure 4 a, b), in the first 50th cycle, the TiO_2 charge and discharge planes have shrunk to about half of their initial length. The LTO/TiO_2-48 had almost no TiO_2 content, so the TiO_2 charge plane was a slope and cannot be distinguished even at the first cycle (Fig. 4 c) discharge plane of TiO_2 in the curve of LTO/TiO_2-48. In $Li_4Ti_5O_{12}$, the lengths of charge and discharge plateaus also reduced in all three samples after the first cycles. Since not all lithium ions inserted in the lattice could be extracted during the discharge process, the length of the plane decreased with cycling [27].

Although the capacity of TiO_2 decayed relatively quicker compared with $Li_4Ti_5O_{12}$, it still provided the valuable capacity to the electrode. As shown in Fig. 5, the first discharge specific capacity of LTO/TiO_2-10 was 181.68 mAh/g, while the LTO/TiO_2-24 had 175.29 mAh/g as initial. On the other hand, the LTO/TiO_2-48, which short in TiO_2 content, have only 154.30 mAh/g for its first cycle. After 100 cycle testing, the capacity for LTO/TiO_2-10, LTO/TiO_2-24, and LTO/TiO_2-48 was 135.16 mAh/g, 142.65 mAh/g, and 121.83 mAh/g. The retentions of the first cycle were 74.7 %, 81.87 %, and 79.32 %, respectively.

The rated capacity is also an essential consideration in lithium-ion batteries. To examine the effect of the different composite electrodes on rate capability, these three Ti-based nanowires studied by charging/discharging at different current rates which were 0.2 C, 0.5 C, 1 C, 2 C, 5 C, 10 C, 20 C, 0.5 C, and 0.2 C. Figure 6 shows LTO/TiO_2-10 has the highest initial capacity, which is 184.75 mAh/g. The initial capacity of LTO/TiO_2-24 was slightly lower than the LTO/TiO_2-10, and it was 177.35 mAh/g. The LTO/TiO_2-48 have the lowest initial capacity. However, at high current rates like 10 C or 20 C, the specific capacity of LTO/TiO_2-10 and LTO/TiO_2-24 seriously hindered, because when it at the high current rate, the spinel TiO_2 stepped to an unstable electrochemical situation and cannot be

fully involved in the electrode reaction.

Furthermore, its crystal structure was more likely to be damaged. Since the $Li_4Ti_5O_{12}$ have good electrochemical stability, when the current rate raised to 10 C and 20 C, the LTO/TiO_2-48 sample has a high specific capacity than the others. After the rate capacity testing, the LTO/TiO_2-10, LTO/TiO_2-24, and LTO/TiO_2-48 have maintained 161.25, 165.25, and 152.53 mAh/g separately. The retentions for each sample were 86.71 %, 92.86 % and 89.79 %, respectively. Theoretically, the LTO/$TiO2$-48 with the lowest TiO_2 content should have the highest retention after the rate test, but there are some other phases of LTO produced during the hydrothermal reaction. These impurities are less electrochemically stable than the pure spinel $Li_4Ti_5O_{12}$. As a result, the rate capacity performance of LTO/TiO_2-48 was worse than it should be.

4. CONCLUSIONS

The LTO/TiO_2 dual-phase nanowires synthesized by hydrothermal reaction. The LTO/TiO_2 nanowires had different morphologies due to various lithiation time. The nanowires initial thickness was around 100 nm, and the 48 h lithiated sample had a thickness of around 200 nm, and the particles almost entirely covered the wires. The XRD results showed that the longer the lithiation time, the LTO levels increased. The first discharge specific capacity of LTO/TiO_2-10, LTO/TiO_2-24, and LTO/TiO_2-48 was 181.68, 175.29 and 154.30 mAh/g, respectively. After the rate capacity testing, the LTO/TiO_2-10, LTO/TiO_2-24, and LTO/TiO_2-48 have maintained 161.25, 165.25, and 152.53 mAh/g separately. The retentions for each sample were 86.71, 92.86 and 89.79 %. Based on the results of electrochemical performance, increased LTO content helped increase the samples cycle stability. However, at 48 h lithiation time also produced impurities, which reduced the cycle stability.

AUTHOR INFORMATION

Corresponding Author

Yillin Fan He — School of Materials Science & Engineering, University of New South Wales, Sydney-2052 (Australia);
Email: hf.yillin@unsw.edu.au

Authors

Dongzhi Yang Chu — School of Materials Science & Engineering, University of New South Wales, Sydney-2052 (Australia);

Zhensheng Zhuo — School of Materials Science & Engineering, University of New South Wales, Sydney-2052 (Australia);

REFERENCES

[1] K. Wu, L. Qian, X. Sun, X. Lei, N. Wu, H. Zhao, and Y. Zhang. (2018). "Cost effective surface passivation film construction on $Li_4Ti_5O_{12}$ anode of lithium ion batteries". *Electrochimica Acta*. **260** : 40–46. 10.1016/j.electacta.2017.11.090.

[2] M. Mancini, F. Nobili, R. Tossici, M. Wohlfahrt-Mehrens, and R. Marassi. (2011). "High performance, environmentally friendly and low cost anodes for lithium-ion battery based on TiO_2 anatase and water soluble binder carboxymethyl cellulose". *Journal of Power Sources*. **196** (22): 9665–9671. 10.1016/j.jpowsour.2011.07.028.

[3] X. Lan, Y. Xin, L. Wang, and X. Hu. (2018). "Nanoscale surface modification of Li-rich layered oxides for high-capacity cathodes in Li-ion batteries". *Journal of Nanoparticle Research*. **20** (3): 80. 10.1007/s11051-018-4165-y.

[4] D. Andre, S. J. Kim, P. Lamp, S. F. Lux, F. Maglia, O. Paschos, and B. Stiaszny. (2015). "Future generations of cathode materials: an automotive industry perspective". *Journal of Materials Chemistry A*. **3** (13): 6709–6732. 10.1039/C5TA00361J.

[5] J. Wang, Y. Yu, B. Li, T. Fu, D. Xie, J. Cai, and J. Zhao. (2015). "Improving the electrochemical properties of $LiNi_{0.5}Co_{0.2}Mn_{0.3}O_2$ at 4.6 v cutoff potential by surface coating with Li_2TiO_3 for lithium-ion batteries". *Physical Chemistry Chemical Physics*. **17** (47): 32033–32043. 10.1039/c5cp05319f.

[6] Z. Guo, Y. Fan, and S. Du. (2018). "Influence of lithium hexafluorophosphate/ethylene carbonate/dimethyl carbonate electrolyte soaking on heat seal strength of polyamide 6/aluminum/cast-polypropylene laminates used as lithium-ion battery packaging". *Journal of Plastic Film and Sheeting*. **34** (1): 10–26. 10.1177/8756087916686141.

[7] J. Shi, N. Ehteshami, J. Ma, H. Zhang, H. Liu, X. Zhang, J. Li, and E. Paillard. (2019). "Improving the graphite/electrolyte interface in lithium-ion battery for fast charging and low temperature operation: Fluorosulfonyl isocyanate as electrolyte additive". *Journal of Power Sources*. **429** : 67–74. 10.1016/j.jpowsour.2019.04.113.

[8] R. Zhao, S. Zhang, J. Liu, and J. Gu. (2015). "A review of thermal performance improving methods of lithium ion battery: Electrode modification and thermal management system". *Journal of Power Sources*. **299** : 557–577. 10.1016/j.jpowsour.2015.09.001.

[9] S. Li and J. Mao. (2018). "The Influence of Different Types of Graphene on the Lithium Titanate Anode Materials of a Lithium Ion Battery". *Journal of Electronic Materials*. **47** (9): 5410–5416. 10.1007/s11664-018-6439-7.

[10] Y. Cai, Y. Huang, W. Jia, X. Wang, Y. Guo, D. Jia, Z. Sun, W. Pang, and Z. Guo. (2016). "Super high-rate, long cycle life of europium-modified, carbon-coated, hierarchical mesoporous lithium-titanate anode materials for lithium ion batteries". *Journal of Materials Chemistry A*. **25** (4): 9949-9957. 10.1039/C6TA03162E.

[11] T. Meng, F. Yi, H. Cheng, J. Hao, D. Shu, S. Zhao, C. He, X. Song, and F. Zhang. (2017). "Preparation of Lithium Titanate/Reduced Graphene Oxide Composites with Three-Dimensional 'Fishnet-Like' Conductive Structure via a Gas-Foaming Method for High-Rate Lithium-Ion Batteries". *ACS Applied Materials & Interfaces*. **9** (49): 42883–42892. 10.1021/acsami.7b15525.

[12] Y. Wang, Y. X. Zhang, W. J. Yang, S. Jiang, X. W. Hou, R. Guo, W. Liu, P. Huang, J. Lu, and H. T. Gu. (2019). "Enhanced Rate Performance of $Li_4Ti_5O_{12}$ Anode for Advanced Lithium Batteries". *Journal of The Electrochemical Society*. **166** (3): A5014–A5018. 10.1149/2.0041903jes.

[13] Q. Tian, P. Chen, Z. Zhang, and L. Yang. (2017). "Achievement of significantly improved lithium storage for novel clew-like

$Li_4Ti_5O_{12}$ anode assembled by ultrafine nanowires". *Journal of Power Sources*. **350** : 49–55. 10.1016/j.jpowsour.2017.03.065.

[14] Z. Chen, H. Li, L. Wu, X. Lu, and X. Zhang. (2018). "$Li_4Ti_5O_{12}$ Anode: Structural Design from Material to Electrode and the Construction of Energy Storage Devices". *Chemical Record*. **18** (3): 350–380. 10.1002/tcr.201700042.

[15] R. Li, W. Xiao, C. Miao, R. Fang, Z. Wang, and M. Zhang. (2019). "Sphere-like SnO_2/TiO_2 composites as high-performance anodes for lithium ion batteries". *Ceramics International*. **45** (10): 13530–13535. 10.1016/j.ceramint.2019.04.059.

[16] K. Amine, I. Belharouak, Z. Chen, T. Tran, H. Yumoto, N. Ota, S. T. Myung, and Y. K. Sun. (2010). "Nanostructured anode material for high-power battery system in electric vehicles". *Advanced Materials*. **22** (28): 3052 –3057. 10.1002/adma.201000441.

[17] Z. Liu, Y. G. Andreev, A. Robert Armstrong, S. Brutti, Y. Ren, and P. G. Bruce (2013). "Nanostructured $TiO_2(B)$: the effect of size and shape on anode properties for Li-ion batteries". *Progress in Natural Science: Materials International*. **23** (3): 235–244. 10.1016/j.pnsc.2013.05.001.

[18] L. Noerochim, R. Fikry, H. Nurdiansah, H. Purwaningsih, A. Subhan, J. Triwibowo, and B. Prihandoko. (2019). "Synthesis of dual-phase $Li_4Ti_5O_{12}$-TiO_2 nanowires as anode for lithium-ion battery". *Ionics*. **25** (4): 1505–1511. 10.1007/s11581-018-2659-3.

[19] B. Shao, X. Yin, W. Hua, Y. Ma, J. Sun, C. Li, D. Chen, D. Guo, and K. Li. (2018). "Synthesis and growth mechanism of sponge-like nickel using a hydrothermal method". *Physica B: Condensed Matter*. **537** : 127–133. 10.1016/j.physb.2018.01.053.

[20] S. Briche, M. Derqaoui, M. Belaiche, E. M. el Mouchtari, P. Wong-Wah-Chung, and S. Rafqah. (2020). "Nanocomposite material from TiO_2 and activated carbon for the removal of pharmaceutical product sulfamethazine by combined adsorption/photocatalysis in aqueous media". *Environmental Science and Pollution Research*. **27** (20): 25523–25534. 10.1007/s11356-020-08939-2.

[21] Q. Guo, Q. Wang, G. Chen, H. Xu, J. Wu, and B. Li. (2016). "Molten Salt Synthesis of Transition Metal Oxides doped $Li_4Ti_5O_{12}$ as Anode Material of Li-Ion Battery". *ECS Transactions*. **72** (9): 11–23. 10.1149/07209.0011ecst.

[22] E. Golestani, M. Javanbakht, H. Ghafarian-Zahmatkesh, H. Beydaghi, and M. Ghaemi. (2018). "Tartaric acid assisted carbonization of $LiFePO_4$ synthesized through in situ hydrothermal process in aqueous glycerol solution". *Electrochimica Acta*. **259** : 903–915. 10.1016/j.electacta.2017.10.123.

[23] A. Lakshmi-Narayana, M. Dhananjaya, N. Guru-Prakash, O. M. Hussain, A. Mauger, and C. M. Julien. (2018). "Li_2TiO_3/Graphene and Li_2TiO_3/CNT Composites as Anodes for High Power Li–Ion Batteries". *ChemistrySelect*. **3** (31): 9150–9158. 10.1002/slct.201801510.

[24] Z. Yang, H. Guo, X. Li, Z. Wang, J. Wang, Y. Wang, Z. Yan, and D. Zhang. (2017). "Graphitic carbon balanced between high plateau capacity and high rate capability for lithium ion capacitors". *Journal of Materials Chemistry A*. **5** (29): 15302–15309. 10.1039/c7ta03862c.

[25] Y. Huang, Y. He, H. Sheng, X. Lu, H. Dong, S. Samanta, H. Dong, X. Li, D. Y. Kim, H. K. Mao, Y. Liu, H. Li, H. Li, and L. Wamg. (2019). "Li-ion battery material under high pressure: Amorphization and enhanced conductivity of $Li_4Ti_5O_{12}$". *National Science Review*. **6** (2): 239–246. 10.1093/nsr/nwy122.

[26] J. Zheng, Z. Yang, Z. He, H. Tong, W. Yu, and J. Zhang. (2018). "In situ formed $LiNi_{0.8}Co_{0.15}Al_{0.05}O_2$@$Li_4SiO_4$ composite cathode material with high rate capability and long cycling stability for lithium-ion batteries". *Nano Energy*. **53** : 613–621. 10.1016/j.nanoen.2018.09.014.

[27] H. Zhou, X. Zhao, C. Yin, and J. Li. (2018). "Regeneration of $LiNi_{0.5}Co_{0.2}Mn_{0.3}O_2$ cathode material from spent lithium-ion batteries". *Electrochimica Acta*. **291** : 142–150. 10.1016/j.electacta.2018.08.134.